Role of cone-beam computed tomography with a large field of view in Goldenhar syndrome

Cosimo Nardi,[a] Luisa De Falco,[a] Valeria Selvi,[a] Chiara Lorini,[b] Linda Calistri,[a] and Stefano Colagrande[a]
Florence, Italy

Introduction: Goldenhar syndrome is a rare disease with hemifacial microsomia and craniofacial disorders originating from the first and second branchial arches, such as ocular, auricular, and vertebral anomalies. The complexity and variety of the ways in which the disease presents itself usually need several examinations. In this study, we aimed to evaluate both craniofacial and vertebral skeletal anomalies and asymmetries between the nonaffected and affected sides in patients with Goldenhar syndrome by using cone-beam computed tomography. **Methods:** Ten patients (7-14 years old; 6 boys, 4 girls) were evaluated via NewTom 5G cone-beam computed tomography (QR srl, Verona, Italy) with a large field of view (18 × 16 cm). Ten anatomic facial landmarks were identified to measure the following distances bilaterally: sella turcica (ST)-mandibular angle, ST-condyle, ST-mastoid, ST-mental foramen, ST-fronto zygomatic suture, ST-zygomatic temporal suture, ST-zygomatic facial foramen, ST-sphenopalatine fossa, mandibular angle-mandibular symphysis, and mandibular angle-condyle. The following 6 volumes were calculated bilaterally: orbit, maxillary sinus, condyle, external ear canal, middle ear, and internal auditory canal. These measurements were performed to assess skeletal asymmetries to compare the nonaffected side with the affected side by the Wilcoxon test. Cervical spine anomalies were classified into fusion anomalies and posterior arch deficiencies. **Results:** All patients showed a deficit of skeletal development on the affected side. Statistically significant differences ($0.001 \leq P$ value ≤ 0.043) between the nonaffected and affected sides were recorded for all measurements, except for ST-frontozygomatic suture, mandibular angle-mandibular symphysis, and maxillary sinus volume. Vertebral fusion anomalies and posterior arch deficiencies were found in 7 and 4 patients, respectively. **Conclusions:** Cone-beam computed tomography with a large field of view was able to accurately identify craniofacial and vertebral skeletal anomalies, and to quantify asymmetries between the nonaffected and affected sides for an efficient maxillofacial treatment planning. (Am J Orthod Dentofacial Orthop 2018;153:269-77)

Oculo-auriculo-vertebral dysplasia is a phenotypically variable developmental anomaly of facial structures originating from the first and second branchial arches.[1,2] In addition to the mandibular and auricular abnormalities, the most severe cases show ocular or vertebral involvements. This is known as the Goldenhar syndrome.[3] The typical presentation of Goldenhar syndrome includes epibulbar dermoids, microtia, vertebral anomalies, and hemifacial microsomia (85% monolateral).[4-7]

Vertebral malformations are mainly represented by vertebral fusions and scoliosis; in the cervical area, they are detected in about half of the patients.[8] Anomalies of the maxillary sinus and inner or medium ear are also frequent, whereas systemic abnormalities and psycho-physical motor underdevelopment are less common.[9,10] The birth prevalence rate varies greatly among authors, ranging from 1 in 5,000 to 1 in 25,000.[11-15] Etiology is multifactorial. It is partly linked to environmental factors during the fetal period, such as smoking, diabetes, and vasoactive drugs, and also partly due to genetic causes. Most chromosomal aberrations are sporadic, whereas only 2% to 10% of them are autosomal dominant or recessive.[10,16]

The complexity and variety of the alterations pose the need for several examinations, such as panoramic

[a]Department of Experimental and Clinical Biomedical Sciences, Radiodiagnostic Unit number 2, University of Florence, Azienda Ospedaliero, Universitaria Careggi, Florence, Italy.
[b]Department of Health Science, University of Florence, Florence, Italy.
All authors have completed and submitted the ICMJE Form for Disclosure of Potential Conflicts of Interest, and none were reported.
Address correspondence to: Cosimo Nardi, Dipartimento di Scienze Biomediche Sperimentali e Cliniche, Radiodiagnostica 2, Università di Firenze, AOU Careggi, Largo Brambilla 3, Firenze, Italia 50134; e-mail, cosimo.nardi@unifi.it.
Submitted, February 2017; revised and accepted, June 2017.
0889-5406/$36.00

https://doi.org/10.1016/j.ajodo.2017.06.024

Table I. Clinical features of the 10 patients

Patient	*Age*	*Sex*	*Hemifacial microsomia*	*Aural abnormalities*	*Eye abnormalities*	*Vertebral abnormalities*
1	7 y 1 mo	M	+	+	+	+
2	8 y 4 mo	M	+	+	+	–
3	9 y 2 mo	M	+	+	–	+
4	14 y 0 mo	F	+	+	+	–
5	13 y 6 mo	F	+	+	–	+
6	10 y 8 mo	F	+	+	–	+
7	11 y 6 mo	M	+	+	+	+
8	8 y 2 mo	M	+	+	+	+
9	7 y 11 mo	F	+	+	+	–
10	7 y 10 mo	M	+	+	–	+

F, Female; *M*, male; +presence; –absence.

radiography, cephalometric and cervical spine x-rays, and sometimes a volumetric imaging technique that allows a detailed analysis of bone structures, such as multislice spiral computed tomography (MSCT).[3,17]

Although magnetic resonance imaging (MRI) does not depict cortical bone well, it has been recently used as an alternative tool[18] because the MSCT of the cervical spine and head delivers a high x-ray radiation dose.[19,20] Nothing has been published about a possible diagnostic role of cone-beam computed tomography (CBCT) in Goldenhar syndrome. This technique provides an adequate volumetric study of the bone structures of the head and neck areas[21] with a high spatial resolution (0.075-0.4 mm isotropic voxel),[22] allowing easy and accurate 2-dimensional and 3-dimensional (3D) measurements.[23] Moreover, it involves relatively low radiation doses compared with MSCT and is only slightly affected by metal artifacts,[24] which often occur in young people with ortho-gnatho-dontic oral metallic treatment. The aims of this retrospective study were to identify craniofacial and vertebral skeletal anomalies and to quantify the asymmetries between the nonaffected and affected sides in patients with Goldenhar syndrome by using CBCT with a large field of view (FOV) as a diagnostic tool.

MATERIAL AND METHODS

From April 2012 to October 2016, 10 patients (6 boys, 4 girls; mean age, 9.9 years) (Table I) affected by Goldenhar syndrome with unilateral craniofacial involvement were examined via CBCT volumetric imaging. This study was approved by the research ethics committee of the University of Florence in Italy, and informed written consent was obtained from each patient. Scans were performed with NewTom 5G (QR srl, Verona, Italy), a horizontal CBCT unit equipped with an amorphous silicon flat-panel detector (20 × 25 cm). The patients lay in a supine position with competent lips and the mouth in habitual occlusion. The same protocol—called "standard regular" by the producer—was used for all examinations. It provided 110 kV, 3.39-5.38 mA, 18 × 16 cm FOV, 18-second scan time, and 3.6-second exposure time with the acquisition of 360 images (1 image for each rotation degree) at the lowest doable automatically set radiation dose. The largest FOV available was chosen to include both the facial skeleton and the vertebral spine up to the sixth cervical vertebra. All CBCT volumes were reconstructed with 0.3-mm isometric voxel size. The 0.4-mm thick axial sections were exported in DICOM format and analyzed by using OsiriX software (version 7.0; OsiriX, Geneva, Switzerland), implemented in a Macintosh operating system with a 21.5-in monitor (Power Macintosh G3; Apple, Cupertino, Calif).

The anatomic points chosen for the 10 linear measurements and the 6 calculated volumes are shown in Figures 1 and 2, respectively. Gonion, pogonion, and zygomatic-facial foramen were identified on the 3D surface-rendering reconstructions. The identification of the remaining 7 points took place on the 2-dimensional reconstruction planes (coronal, sagittal, and axial) by using the 3D multiplanar reconstruction function that allowed the simultaneous display of any structure on those 3 planes. The distances between sella turcica and the other points, except for pogonion, were calculated by the 3D curved multiplanar reconstruction function. The distances between gonion and pogonion and between gonion and the condyle were calculated also. The last 2 corresponded with the length of the mandibular body and the mandibular ramus, respectively.

Orbit, maxillary sinus, and condyle volumes were measured on the axial images, whereas the external ear canal, middle ear, and internal auditory canal volumes were measured on the coronal images. All volumes were calculated using the volume region of interest function after a region of interest surrounding the anatomic structures was depicted in each slice in which the same structures could be seen.

Fig 1. The 10 anatomic points used for the linear measurements: **A** and **B,** sagittal planes; **C** and **D,** axial planes; **E,** coronal plane; **F,** 3D volume rendering. Note the fusion of the vertebral bodies and os odontoideum (*circle*). *ST*, Center of sella turcica; *PO*, most anterior point of the mandibular symphysis or pogonion; *GO*, midpoint of the posterior margin of the mandibular angle or gonion; *CO*, most cranial point of the mandibular condyle; *ZTS*, midpoint of the zygomatic-temporal suture; *ZFF*, zygomatic-facial foramen; *FZS*, midpoint of the frontozygomatic suture; *SPF*, most caudal point of the sphenopalatine fossa; *MF*, mental foramen; *MA*, most caudal point of the mastoid.

The cervical vertebrae anomalies were assessed by adaptation of the conventional x-ray classification of Sandham[25] to CBCT. Sandham divided the vertebral anomalies into 2 groups: fusion anomalies and posterior arch deficiencies. Fusion anomalies were defined as incomplete separation with osseous continuities between 2 vertebral bodies or arches. Posterior arch deficiencies were represented by a discontinuity or interruption of the posterior arch of the vertebra due to incomplete ossification or dehiscence.

All examinations were evaluated by 3 skilled maxillofacial imaging observers (S.C., C.N., V.S.) (with 21, 10, and 4 years of experience, respectively). The assessment was carried out twice by each observer, with an interval of 3 months. Collected data were analyzed using SPSS statistical analysis software (version 23.0; IBM, Armonk, NY). Intraobserver and interobserver reliability values were determined for each designated parameter (affected side, nonaffected side, reduction factor, and differences between the nonaffected and the affected sides). For both linear and volumetric measurements, the intraclass correlation coefficient was used. According to Zidan et al,[26] intraclass correlation coefficient values of 0.00 to 0.10, 0.11 to 0.40, 0.41 to 0.60, 0.61 to 0.80, and 0.81 to 1.0 represent no, slight, fair, good, and very good agreement, respectively.

The mean, median, standard deviation, and maximum and minimum values of each parameter were calculated for both linear and volumetric measurements among the 60 observations (2 evaluations by 3 observers for 10 patients). The reduction factor was the ratio between the nonaffected and affected sides as stated by Hirschfelder et al.[6] Then, a descriptive analysis was performed. The differences between the nonaffected and affected sides for all linear and volumetric measurements were assessed by using the Wilcoxon signed rank test for paired data. For each analysis, a P value ≤ 0.05 was considered to be statistically significant.

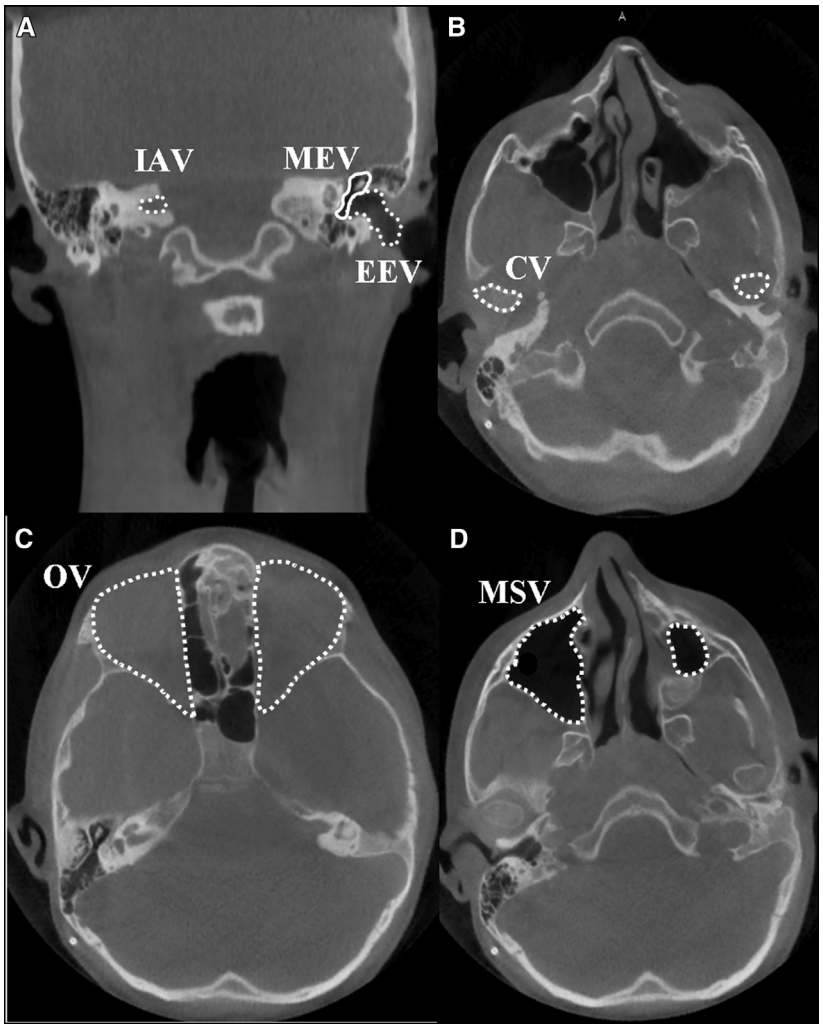

Fig 2. Single-slice volume contouring drawn for volumetric measurements: **A,** coronal plane; **B-D,** axial planes. *EEV*, External ear canal volume, calculated from the inner border of the tragus to the tympanic membrane; *MEV*, middle ear volume, defined by the bone walls of the tympanic cavity; *IAV*, Internal auditory canal volume, calculated from the inner acoustic foramen to the sickle crest; *CV*, condyle volume, inferiorly delimited by a plane passing through the most caudal point of the mandibular notch and perpendicular to the tangent of the mandibular ramus; *OV*, orbit volume, defined by its bone borders and posteriorly by the optic foramen; *MSV*, maxillary sinus volume, defined by its bone walls.

RESULTS

Alterations of bone development were detected on the affected side in all 10 patients (Tables II and III). Statistically significant differences ($0.001 \leq P$ value ≤ 0.043) between the nonaffected and affected sides were observed for all linear and volumetric measurements, except for maxillary sinus volume and the distances between gonion and pogonion, and between sella turcica and the fronto-zygomatic suture ($P = 0.5$). Intraobserver and interobserver reliabilities for both linear and volumetric measurements were very good. The intraclass correlation coefficient values were 0.84 ± 0.26 and 0.83 ± 0.28 for the linear measurements, respectively, and 0.96 ± 0.08 and 0.91 ± 0.13 for the volumetric measurements, respectively.

Among the distances with a statistically significant difference between the 2 sides, the highest value of the reduction factor (mean, 1.40; median, 1.29; SD, 0.36) was found in the distance between gonion and the condyle. All remaining distances had mean and median reduction factors close to 1 and very similar to each other (ranging from 1.05 to 1.15 and from 1.02 to 1.09, respectively). This demonstrated that the asymmetry between the 2 sides was substantial for the mandibular

Table II. Linear measurements

Distance	Parameter	Mean (cm)	Median (cm)	SD (cm)	Minimum (cm)	Maximum (cm)
GO-CO	NAS	4.96	4.86	0.79	4.09	6.25
	AS	3.69	3.77	0.90	2.42	4.94
	RF	1.40	1.29	0.36	1.08	2.02
	DIF	1.27	1.19	0.77	0.31	2.47
GO-PO	NAS	7.85	7.53	0.96	7.07	9.51
	AS	7.81	7.43	1.10	6.65	9.39
	RF	1.01	1.01	0.08	0.91	1.12
	DIF	0.04	0.10	0.57	−0.77	0.81
ST-CO	NAS	5.50	5.60	0.19	5.17	5.63
	AS	4.89	5.10	0.73	3.83	5.54
	RF	1.15	1.02	0.20	1.01	1.46
	DIF	0.60	0.12	0.76	0.07	1.77
ST-GO	NAS	7.68	7.37	0.85	6.75	9.03
	AS	7.09	6.84	0.92	6.11	8.60
	RF	1.09	1.08	0.05	1.04	1.16
	DIF	0.59	0.53	0.32	0.25	1.10
ST-ZTS	NAS	6.07	6.20	0.25	5.67	6.26
	AS	5.75	5.76	0.28	5.34	6.13
	RF	1.06	1.06	0.04	1.01	1.10
	DIF	0.31	0.32	0.20	0.07	0.55
ST-FZS	NAS	6.36	6.38	0.71	5.22	7.16
	AS	6.47	6.60	0.45	5.77	6.91
	RF	0.98	0.96	0.06	0.91	1.05
	DIF	−0.11	−0.24	0.39	−0.54	0.34
ST-ZFF	NAS	6.59	6.44	0.68	5.63	7.39
	AS	6.29	6.25	0.72	5.46	7.20
	RF	1.05	1.03	0.04	1.03	1.12
	DIF	0.31	0.19	0.22	0.17	0.68
ST-MA	NAS	7.53	7.55	0.17	7.38	7.78
	AS	6.82	7.13	0.66	5.72	7.35
	RF	1.11	1.05	0.11	1.03	1.29
	DIF	0.71	0.32	0.64	0.22	1.67
ST-MF	NAS	8.81	8.85	0.91	7.51	9.97
	AS	8.42	7.98	1.02	7.45	9.86
	RF	1.05	1.02	0.06	1.01	1.15
	DIF	0.40	0.15	0.46	0.06	1.14
ST-SPF	NAS	3.60	3.65	0.41	2.98	4.13
	AS	3.25	3.30	0.23	2.86	3.48
	RF	1.11	1.09	0.06	1.04	1.19
	DIF	0.35	0.30	0.21	0.12	0.65

For each of the 10 distances, the mean, median, standard deviation, and minimum and maximum values were calculated for the nonaffected side, the affected side, the reduction factor, and the difference between the 2 sides.
NAS, Nonaffected side; *AS*, affected side; *RF*, reduction factor (nonaffected side/affected side); *DIF*, difference between the 2 sides (nonaffected side–affected side). Refer to Figure 1 for the acronyms of the distances.

ramus and mild for all remaining distances. The mean differences between the nonaffected and affected sides for the distances between sella turcica and gonion, sella turcica and the condyle, and sella turcica and the mastoid were 0.59, 0.60, and 0.71 with standard deviations of 0.32, 0.76, and 0.64, respectively. These values showed that these distances had high variability in our series.

Table III. Volumetric measurements

Volume	Parameter	Mean (cm^3)	Median (cm^3)	SD (cm^3)	Minimum (cm^3)	Maximum (cm^3)
OV	NAS	22.08	21.73	1.29	20.33	23.51
	AS	20.06	19.86	1.74	18.51	22.83
	RF	1.10	1.10	0.05	1.03	1.16
	DIF	2.02	1.87	0.91	0.68	2.94
MSV	NAS	11.96	11.55	3.29	8.53	17.25
	AS	10.07	10.45	4.71	3.38	16.40
	RF	1.53	1.01	1.17	0.98	3.63
	DIF	1.89	0.12	3.94	−0.26	8.89
CV	NAS	1.13	1.13	0.42	0.54	1.72
	AS	0.48	0.29	0.49	0.08	1.34
	RF	4.89	2.71	5.56	1.29	14.69
	DIF	0.66	0.71	0.34	0.27	1.12
EEV	NAS	0.66	0.63	0.18	0.44	0.91
	AS	0.22	0.24	0.23	0.01	0.56
	RF	30.31	2.55	41.00	1.13	91.00
	DIF	0.44	0.46	0.32	0.08	0.91
MEV	NAS	0.45	0.44	0.06	0.37	0.52
	AS	0.14	0.02	0.21	0.01	0.51
	RF	24.25	23.88	22.76	1.02	50.00
	DIF	0.31	0.39	0.20	0.01	0.50
IAV	NAS	0.20	0.20	0.05	0.13	0.26
	AS	0.16	0.17	0.06	0.10	0.22
	RF	1.31	1.28	0.26	1.03	1.72
	DIF	0.04	0.03	0.03	0.01	0.07

For each of the 6 volumes, the mean, median, standard deviation, and minimum and maximum values were calculated for the nonaffected side, the affected side, the reduction factor, and the difference between the 2 sides.
NAS, Nonaffected side; *AS*, affected side; *RF*, reduction factor (nonaffected side/affected side); *DIF*, difference between the 2 sides (nonaffected side–affected side). Refer to Figure 2 for the acronyms of the volumes.

Among the volumes with a statistically significant difference between the 2 sides, the mean reduction factor for the external ear canal, middle ear, and condyle volumes were 30.31, 24.25, and 4.89 with standard deviations of 41.00, 22.76, and 5.56, respectively. The mean values proved the high variability between the nonaffected and affected sides, whereas the standard deviation values proved the high interpatient variability. Conversely, the orbit and internal auditory canal volumes had mean reduction factors of 1.10 and 1.31 with standard deviations of 0.05 to 0.26, respectively. It proved little variability both between the nonaffected and affected sides, and among the different patients. Seven of the 10 patients were found to have cervical spine abnormalities (Table IV). Four of them had both fusion anomalies on the same side as the hemifacial microsomia and posterior arch deficiencies. Posterior arch deficiencies corresponded with the vertebral clefts, whereas the fusion anomalies included the fusion of vertebral arches and the failure of the segmentation of the vertebral bodies with interbody fusions. The other

Table IV. Vertebral fusion anomalies (FUS) and posterior arch deficiencies (PAD) of the 10 patients

Patient	*FUS*	*PAD*
1	C3-C4 arches (left) C5-C6 bodies (left)	C1, C3, C4, C5
2		
3	C5-C6 bodies (left)	C5, C6
4		
5	C2-C3 bodies (bilateral) C4-C5-C6 bodies (bilateral)	
6	C2-C3 bodies (left)	C4, C5
7	C3-C4-C5 bodies (bilateral)	
8	C2-C3 bodies (right) C2-C3-C4 arches (right)	C2-C3-C4
9		
10	C2-C3-C4 bodies (bilateral)	

3 patients had bilateral fusion anomalies without posterior arch deficiencies.

DISCUSSION

The wide spectrum of Goldenhar syndrome skeletal alterations requires several different x-ray examinations such as panoramic radiography, and cephalometric and cervical spine x-rays. Since MRI does not show cortical bone with accuracy, MSCT is currently considered the volumetric imaging gold standard for these patients. Nevertheless, in clinical practice, children are seldom subjected to MSCT for radioprotection reasons. We hypothesized that CBCT could be a solution to the high radiation dose problem in young patients since it is a low-dose volumetric imaging technique with excellent performance for bone structure analysis.

In our series, the distance between gonion and the condyle had the highest mean and standard deviation values of the reduction factor. The same was observed for the external ear canal volume and the middle ear volume. On the contrary, the distance between gonion and pogonion, between sella turcica and the fronto-zygomatic suture, and the maxillary sinus volume were the only 3 measurements with no statistically significant differences between the nonaffected and affected sides.

The high values of the reduction factor for the distance between gonion and the condyle indicated the greatest asymmetry between the nonaffected and affected sides. It proved that the small length of the mandibular ramus of the affected side was the main reason for hemifacial microsomia. All the other statistically significant linear measurements showed reduction factor values close to 1 and almost equal to each other, indicating that a slight degree of asymmetry between the 2 sides was recognizable. Among the measurements in which statistically significant differences between the 2 sides were not observed, the mandibular body—represented by the distance between gonion and pogonion—showed median values similar to those between the nonaffected (7.53 cm) and affected (7.43 cm) sides. Analogous results were found by Shibazaki-Yorozuya et al[27] in patients with hemifacial microsomia. They noticed that the mandibular ramus was shorter, whereas the mandibular body could be equal, shorter, or longer on the affected side than on the nonaffected side. Since the mandibular ramus was shorter, the mandibular angle assumed a different position between the 2 sides. As studied by Yañez-Vico et al,[28] the mandibular angle was situated anteriorly and medially from the affected side in patients with craniofacial asymmetry. Regarding maxillary sinus volume, Wink et al[29] also stated that patients affected by hemifacial microsomia had no significant abnormalities and no differences between maxillary sinuses, although the upper jaws could be altered. They supposed that it was because the development of the maxillary bone and the maxillary sinus took place mostly at 2 different times, in the womb and after birth, respectively.

The distance between sella turcica and the fronto-zygomatic suture was the only result in this study that was inconsistent with previous studies. Manara et al[3] stated that there was a statistically significant difference between patients with oculo-auriculo-vertebral dysplasia and the controls for the above-mentioned distance. Unlike the zygomatic bone, the frontal bone does not develop from one of the branchial arches, which appears altered in Goldenhar syndrome. In our opinion, the different embryologic origin of the zygomatic bone and the frontal bone is the basis of the high variability of the fronto-zygomatic suture location.[16] Therefore, this anatomic landmark either was not involved or was involved to a different extent in our series, unlike that of Manara et al. Furthermore, in our series, the different alterations did not inevitably coexist in the same patient. They could range from mild to severe forms. This was consistent with the high phenotypic heterogeneity widely described in the literature.[10] There is no agreement among authors on the definition of the minimum disease criteria.[3-7,11-15,17]

The high variability of the craniofacial skeletal alterations among the patients was proved by the high standard deviation values of the reduction factors of most of the measurements. It was particularly clear for the external ear canal and the middle ear volumes because total atresia of the external ear canal and agenesis of the ossicular chain were detected in some patients, whereas only neurosensorial hypoacusis was found in others.

Vertebral malformations were found in 7 patients. Three of them had bilateral fusion anomalies, and 4 had monolateral fusion anomalies combined with

posterior arch deficiencies. In addition, 1 patient had os odontoideum, which is characterized by a congenital abnormality of the second cervical vertebra, in which the odontoid process is detached from the vertebral body by a transverse gap (Fig 1). Hypoplasia of the odontoid process, described by other authors in Goldenhar syndrome, was not observed in our patients.[30]

In orthodontics, correct and precise measurements of distances, angles, and volumes are essential for both an initial framework and follow-up of craniofacial malformations. Panoramic radiography and cephalometric x-rays have significant limitations because of the 2-dimensional representation of 3D structures, anatomic noise, superimposition, and geometric distortion effect. Therefore, accurate measurements can only be achieved by using volumetric imaging technique such as CBCT or MSCT.

In general terms, both of these techniques use the same image reconstruction principle, termed back projection, with the addition of the algorithm of Feldkamp et al[31] in CBCT. MSCT is characterized by higher milliamperes, a wider dynamic range, and greater contrast and temporal resolution than CBCT.[32] MSCT is available in all developed countries; it allows good detection of soft tissues and is commonly used for contrast-enhanced examinations.[33] CBCT has greater spatial resolution than MSCT, although CBCT image quality is partially degraded by scattered radiation since there is no postpatient collimation.[32] In the head scan, the effective doses of MSCT and CBCT are 1892 and 249 μSv, respectively, whereas in the cervical spine scan, the effective doses of MSCT and CBCT are 3409 and 248 μSv, respectively.[20] Effective doses of panoramic radiography, cephalometric x-rays (2 projections), and cervical spine x-rays (2 projections) are 15 μSv,[34] 6 μSv,[34] and 60 μSv,[35] respectively. Moreover, CBCT has lower mean technical and operating costs per procedure, approximately $70 and $175 for CBCT and unenhanced MSCT, respectively.[36,37]

In our series, CBCT with head and neck FOV appeared to be a volumetric imaging technique capable of assessing craniofacial and cervical skeletal structures simultaneously, with a noteworthy reduction of radiation dose. Therefore, CBCT could be considered the most suitable alternative for detecting skeletal alterations in Goldenhar syndrome. We believe that CBCT could even become the elective imaging technique in medical follow-ups and surgical workups of these patients because of its reduced radiation dose, relatively low cost, high image quality, and limited metal artifacts.[22,24]

With this background, we believe that CBCT could and should be recommended in congenital craniocervical malformations and maxillofacial pediatric diseases with prevalent bone expression such as cleft lip and palate, Wildervanck syndrome, and oculo-auriculo-vertebral, septo-optic, and oto-mandibular dysplasias. Further studies should investigate the helpfulness of CBCT in these malformations.

CBCT proved to be inadequate for soft tissue evaluation and especially in the study of masticatory muscles that are typically altered in hemifacial microsomia.[38] Ultrasound is an accurate and innocuous tool for measuring the thickness of masticatory muscles.[39] Nevertheless, MRI is the gold standard in the analysis of soft tissues. Recently, a novel software based on the fused images of soft and hard tissues, called multimodality MRI-CBCT image registration, was tested.[40] We believe that this resource could be helpful in the study of craniofacial disorders.

In addition, CBCT cannot replace dynamic x-ray examinations in the study of cervical instability, which may be life threatening during general anesthesia.[30]

Two of the 10 examinations had to be repeated because of patient movements. This is not an inconsiderable aspect, since another weak point of CBCT is its long scan times, ranging from 5.4 to 40 seconds (18 seconds in our study).[41] Therefore, the possibility of motion artifacts cannot be ignored in pediatric patients because taking the examination twice means a double radiation dose.[24,42] To reduce repetition of examinations, further studies should both examine means of head/chin/mouth/jaws restraint and test software for mathematic algorithms capable of correcting images impaired during patient movement.

In this study, there were not enough patients for a definite judgment about the efficacy of CBCT in Goldenhar syndrome. This was a pilot study to determine whether additional research with larger population samples is needed or whether CBCT plays no role in this. Goldenhar syndrome is rare, and it is difficult to enroll a large number of patients. The original articles assessing this syndrome by x-rays or MSCT analyzed 11.6 subjects on average.[7,8,18,43-45] Another possible weakness common to all studies about hemifacial microsomia is a lack of reference values to qualify facial asymmetries as physiological or pathological. This is usually related to the clinical opinion and the individual perception of the patient.[46] Lastly, no comparison between CBCT and MSCT was performed. Comparative studies carried out in young people in which both techniques used ionizing radiation are hard to ethically justify.

CONCLUSIONS

In our series, a low-dose 3D imaging technique such as CBCT with a large FOV was able to (1) accurately identify craniofacial and vertebral skeletal

anomalies at 1 time, and (2) quantify the asymmetries between the nonaffected and affected sides in patients with Goldenhar syndrome, providing quantitative data appropriate for maxillofacial medical or surgical planning.

REFERENCES

1. Hennersdorf F, Friese N, Löwenheim H, Tropitzsch A, Ernemann U, Bisdas S. Temporal bone changes in patients with Goldenhar syndrome with special emphasis on inner ear abnormalities. Otol Neurotol 2014;35:826-30.
2. Ashokan CS, Sreenivasan A, Saraswathy GK. Goldenhar syndrome—review with case series. J Clin Diagn Res 2014;8:ZD17-19.
3. Manara R, Schifano G, Brotto D, Mardari R, Ghiselli S, Gerunda A, et al. Facial asymmetry quantitative evaluation in oculoauriculovertebral spectrum. Clin Oral Investig 2016;20:219-25.
4. Shrestha UD, Adhikari S. Craniofacial microsomia: Goldenhar syndrome in association with bilateral congenital cataract. Case Rep Ophthalmol Med 2015;2015:435967.
5. Vinay C, Reddy RS, Uloopi KS, Madhuri V, Sekhar RC. Craniofacial features in Goldenhar syndrome. J Indian Soc Pedod Prev Dent 2009;27:121-4.
6. Hirschfelder U, Piechot E, Schulte M, Leher A. Abnormalities of the TMJ and the musculature in the oculo-auriculo-vertebral spectrum (OAV). A CT study. J Orofac Orthop 2004;65:204-16.
7. Martelli H Jr, Miranda RT, Fernandes CM, Bonan PR, Paranaíba LM, Graner E, et al. Goldenhar syndrome: clinical features with orofacial emphasis. J Appl Oral Sci 2010;18:646-9.
8. Avon SW, Shively JL. Orthopaedic manifestations of Goldenhar syndrome. J Pediatr Orthop 1988;8:683-6.
9. Tasse C, Böhringer S, Fischer S, Lüdecke HJ, Albrecht B, Horn D, et al. Oculo-auriculo-vertebral spectrum (OAVS): clinical evaluation and severity scoring of 53 patients and proposal for a new classification. Eur J Med Genet 2005;48:397-411.
10. Beleza-Meireles A, Clayton-Smith J, Saraiva JM, Tassabehji M. Oculo-auriculo-vertebral spectrum: a review of the literature and genetic update. J Med Genet 2014;51:635-45.
11. Araneta MR, Moore CA, Olney RS, Edmonds LD, Karcher JA, McDonough C, et al. Goldenhar syndrome among infants born in military hospitals to Gulf War veterans. Teratology 1997;56:244-51.
12. Grabb WC. The first and second branchial arch syndrome. Plast Reconstr Surg 1965;36:485-508.
13. Harris J, Kallen B, Robert E. The epidemiology of anotia and microtia. J Med Genet 1996;33:809-13.
14. Mastroiacovo P, Corchia C, Botto LD, Lanni R, Zampino G, Fusco D. Epidemiology and genetics of microtia-anotia: a registry based study on over one million births. J Med Genet 1995;32:453-7.
15. Morrison PJ, Mulholland HC, Craig BG, Nevin NC. Cardiovascular abnormalities in the oculoauriculo-vertebral spectrum (Goldenhar syndrome). Am J Med Genet 1992;44:425-8.
16. Passos-Bueno MR, Ornelas CC, Fanganiello RD. Syndromes of the first and second pharyngeal arches: a review. Am J Med Genet A 2009;149:1853-9.
17. Saccomanno S, Greco F, D'Alatri L, De Corso E, Pandolfini M, Sergi B, et al. Role of 3D-CT for orthodontic and ENT evaluation in Goldenhar syndrome. Acta Otorhinolaryngol Ital 2014;34:283-7.
18. Manara R, Brotto D, Ghiselli S, Mardari R, Toldo I, Schifano G, et al. Cranial nerve abnormalities in oculo-auriculo-vertebral spectrum. AJNR Am J Neuroradiol 2015;36:1375-80.
19. Okano T, Harata Y, Sugihara Y, Sakaino R, Tsuchida R, Iwai K, et al. Absorbed and effective doses from cone beam volumetric imaging for implant planning. Dentomaxillofac Radiol 2009;38:79-85.
20. Nardi C, Talamonti C, Pallotta S, Saletti P, Calistri L, Cordopatri C, et al. Head and neck effective dose and quantitative assessment of image quality: a study to compare cone beam CT and multislice spiral CT. Dentomaxillofac Radiol 2017;46:20170030.
21. Liang X, Jacobs R, Hassan B, Li L, Pauwels R, Corpas L, et al. A comparative evaluation of cone beam computed tomography (CBCT) and multi-slice CT (MSCT). Part I. On subjective image quality. Eur J Radiol 2010;75:265-9.
22. Watanabe H, Honda E, Tetsumura A, Kurabayashi T. A comparative study for spatial resolution and subjective image characteristics of a multi-slice CT and a cone-beam CT for dental use. Eur J Radiol 2011;77:397-402.
23. Liang X, Lambrichts I, Sun Y, Denis K, Hassan B, Li L, et al. A comparative evaluation of cone beam computed tomography (CBCT) and multi-slice CT (MSCT). Part II: on 3D model accuracy. Eur J Radiol 2010;75:270-4.
24. Nardi C, Borri C, Regini F, Calistri L, Castellani A, Lorini C, et al. Metal and motion artifacts by cone beam computed tomography (CBCT) in dental and maxillofacial study. Radiol Med 2015;120:618-26.
25. Sandham A. Cervical vertebral anomalies in cleft lip and palate. Cleft Palate J 1986;23:206-14.
26. Zidan M, Thomas RL, Slovis TL. What you need to know about statistics, part II: reliability of diagnostic and screening tests. Pediatr Radiol 2015;45:317-28.
27. Shibazaki-Yorozuya R, Yamada A, Nagata S, Ueda K, Miller AJ, Maki K. Three-dimensional longitudinal changes in craniofacial growth in untreated hemifacial microsomia patients with cone-beam computed tomography. Am J Orthod Dentofacial Orthop 2014;145:579-94.
28. Yáñez-Vico RM, Iglesias-Linares A, Torres-Lagares D, Gutiérrez-Pérez JL, Solano-Reina E. Three-dimensional evaluation of craniofacial asymmetry: an analysis using computed tomography. Clin Oral Investig 2011;15:729-36.
29. Wink JD, Paliga JT, Tahiri Y, Goldstein JA, Taylor JA, Bartlett SP. Maxillary involvement in hemifacial microsomia: an objective three-dimensional analysis of the craniofacial skeleton. J Craniofac Surg 2014;25:1236-40.
30. Healey D, Letts M, Jarvis JG. Cervical spine instability in children with Goldenhar's syndrome. Can J Surg 2002;45:341-3.
31. Feldkamp LA, Davis LC, Kress JW. Practical cone-beam algorithm. J Opt Soc Am A 1984;1:612-9.
32. Pauwels R, Beinsberger J, Stamatakis H, Tsiklakis K, Walker A, Bosmans H, et al. Comparison of spatial and contrast resolution for cone-beam computed tomography scanners. Oral Surg Oral Med Oral Pathol Oral Radiol 2012;114:127-35.
33. Kim KD, Ruprecht A, Wang G, Lee JB, Dawson DV, Vannier MW. Accuracy of facial soft tissue thickness measurements in personal computer-based multiplanar reconstructed computed tomographic images. Forensic Sci Int 2005;155:28-34.
34. Harris D, Horner K, Gröndahl K, Jacobs R, Helmrot E, Benic GI, et al. E.A.O. guidelines for the use of diagnostic imaging in implant dentistry 2011. A consensus workshop organized by the European Association for Osseointegration at the Medical University of Warsaw. Clin Oral Implants Res 2012;23:1243-53.
35. Ben-Shlomo A, Bartal G, Mosseri M, Avraham B, Leitner Y, Shabat S. Effective dose reduction in spine radiographic imaging by choosing the less radiation-sensitive side of the body. Spine J 2016;16:558-63.
36. Saini S, Sharma R, Levine LA, Barmson RT, Jordan PF, Thrall JH. Technical cost of CT examinations. Radiology 2001;218:172-5.

37. Christell H, Birch S, Hedesiu M, Horner K, Ivanauskaité D, Nackaerts O, et al. Variation in costs of cone beam CT examinations among healthcare systems. Dentomaxillofac Radiol 2012; 41:571-7.
38. Huisinga-Fischer CE, Zonneveld FW, Vaandrager JM, Prahl-Andersen B. Relationship in hypoplasia between the masticatory muscles and the craniofacial skeleton in hemifacial microsomia, as determined by 3-D CT imaging. J Craniofac Surg 2001;12:31-40.
39. Castelo PM, Pereira LJ, Andrade AS, Marquezin MC, Gavião MB. Evaluation of facial asymmetry and masticatory muscle thickness in children with normal occlusion and functional posterior crossbite. Minerva Stomatol 2010;59:423-30.
40. Al-Saleh MA, Punithakumar K, Lagravère M, Boulanger P, Jaremko JL, Major PW. Three-dimensional assessment of temporomandibular joint using MRI-CBCT image registration. PLoS One 2017;12:e0169555.
41. Nemtoi A, Czink C, Haba D, Gahleitner A. Cone beam CT: a current overview of devices. Dentomaxillofac Radiol 2013;42:20120443.
42. Nardi C, Molteni R, Lorini C, Taliani GG, Matteuzzi B, Mazzoni E, et al. Motion artefacts in cone beam CT: an in vitro study about the effects on the images. Br J Radiol 2016;89:20150687.
43. Anderson PJ, David DJ. Spinal anomalies in Goldenhar syndrome. Cleft Palate Craniofac J 2005;42:477-80.
44. Cingano L, Cohen E, Cohen A, Giordanetto J, Loria P, Calcagno E. Odontostomatological aspects in patients with Goldenhar syndrome: a series of 9 patients. Minerva Stomatol 2013;62:375-85.
45. Al Kaissi A, Ben Chehida F, Ganger R, Klaushofer K, Grill F. Distinctive spine abnormalities in patients with Goldenhar syndrome: tomographic assessment. Eur Spine J 2015;24:594-9.
46. Yañez-Vico RM, Iglesias-Linares A, Torres-Lagares D, Gutiérrez-Pérez JL, Solano-Reina E. Diagnostic of craniofacial asymmetry. Literature review. Med Oral Patol Oral Cir Bucal 2010;15:494-8.